Sensors and Materials, Vol. 17, No. 8 (2005) 453–463
MYU Tokyo

S & M 0623

A Single-Axis Thermal Convective Gas Gyroscope

Van Thanh Dau*, Dzung Viet Dao[1], Tatsuo Shiozawa[2]
Hideo Kumagai[2] and Susumu Sugiyama

Graduate School of Science and Engineering, Ritsumeikan University
[1]Center for Promotion of the 21st Century COE Program, Ritsumeikan University
1-1-1 Noji-Higashi, Kusatsu-shi, Shiga 525-8577, Japan
[2]Guidance and Navigation Section, Tamagawa Seiki Co., Ltd.
1879 Oyasumi, Iida-shi, Nagano 395-8515, Japan

(Received January 14, 2005; accepted June 27, 2005)

Key words: gas gyroscope, thermal convective, thermoresistive effect

In this paper, the design, simulation and fabrication of a single axis semiconductor gas gyroscope are presented. The sensor configuration consists of a piezoelectric pump and a micro-thermal-sensing element packaged in an aluminum case with diameter and length of 14 mm and 25 mm, respectively. This gas gyroscope utilizes thermal convective transfer and the thermoresistive effect of Si to detect the applied angular rate. Good agreement between the results of sensitivity simulations and the experimental data has been realized. The sensitivity is 0.15 mV/deg/s, which is 62 times higher than that of a gas gyroscope of the same design but with tungsten as the sensing element. Moreover, the power consumption of this gyroscope is only 5.5 mW, i.e. one fourth of that of the gyroscope with tungsten. Nonlinearity is 0.5% FSO, and the crosstalk is 0.5%. The resolution based on sensitivity and noise analyses (i.e., thermal noise and 1/*f* noise in the thermistors) is 0.04°/s.

1. Introduction

The proposed gas gyroscope is based on the hot-wire anemometer making use of the thermoresistive effect of a silicon thermistor wire. Unlike vibrating gyroscopes reported in recent micro-electro-mechanical systems (MEMS),[1–3] our gas gyroscope has no moving mass; this eliminates the inherent problems which usually occur in vibrating gyroscopes, such as potential fragility, low shock resistance, squeezed-film air damping, and vibration noise from the driving mode to the sensing mode.

*Corresponding author, e-mail address: gr023023@se.ritsumei.ac.jp

Hot-wire anemometers have been used widely as research tools in fluid mechanics and have also been developed as gas sensors because of their reliable detection of fluctuation amounting to only a few percent of mean flow velocity.[9,12,14,15] Other recent applications of this technique are in thermal accelerometers and thermal inclinometers.[4–6] These kinds of sensors are simple, reliable, and have high sensitivity.

A gas gyroscope with wires made of tungsten has been fabricated and commercialized. However, the metallic sensing element has a temperature coefficient of resistance (TCR) much smaller than that of lightly doped silicon[11] and its fabrication is not adaptable to the batch processing in MEMS technology.

In this study, a silicon micro-thermistor wire or silicon hot wire, hereinafter called a thermistor, is used as the sensing part of the gyroscope. The design and fabrication of the thermistor, the simulation of gas flow, and the heat convection transfer problem are presented. The shock resistance is also simulated up to 3000 g (g is gravitational acceleration).

2. Sensor Design and Operating Principle

The gyroscope configuration, as shown schematically in Fig. 1, consists of two main parts packaged in an aluminum case with a diameter and length of 14 mm and 25 mm, respectively. The first part is a piezoelectric diaphragm pump, which oscillates at a frequency of 7 kHz to create a continuous gas flow; the peak flow velocity measured at the sensing element is 3.5 m/s. The pump is the only moving part of the sensor and has been tested for a very long performance life.

The second main part is the thermistor, the working principle of which is based on the thermoresistive effect in silicon. The thermistor is made of lightly doped p-type silicon and is placed 7.5 mm downstream of the nozzle orifice. To detect the angular rate, two thermistors are arranged opposite each other in the same plane. Each thermistor is a p-type silicon wire with the dimensions of $400 \times 4 \times 2\ \mu m^3$ (length × width × thickness). These thermistors are connected to form one Wheatstone half-bridge.

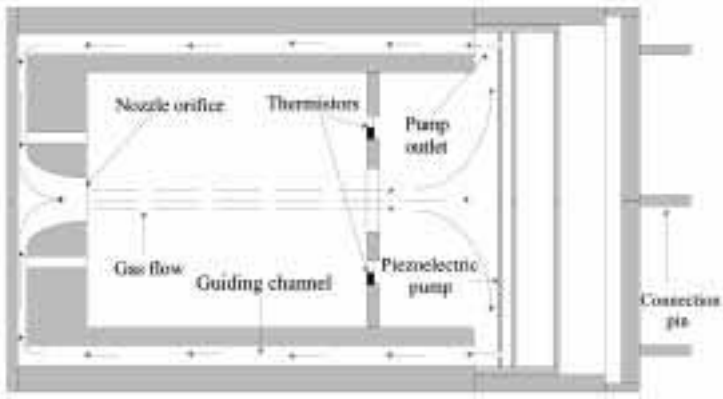

Fig. 1. Schematic view of the sensor configuration.

Inert neon gas was used in this study because its thermal conductivity is two times higher than that of air. The gas, under high pressure from pump vibration at the end of the sensor, is forced to flow through four guiding circular channels to the chamber at the other end. The flow is reversed and directed via the nozzle orifice. Then the gas moves toward the sensing element through the symmetric center between the two thermistors perpendicular to their plane. The entire flow finally returns to the pump chamber to complete the circulation cycle.

As an angular rate is applied, the gas flow direction is deflected due to Coriolis acceleration. This causes the opposite cooling effect between the two opposing thermistors and, as a result, the resistances of the two thermistors change in opposite directions. This resistance change is then converted to an output voltage change by the Wheatstone bridge. The working principle is shown schematically in Fig. 2.

The magnitude and direction of the deflection are calculated using the conventional mathematical expression for Coriolis acceleration:

$$\vec{a}_C = 2\vec{\omega} \times \vec{V}, \tag{1}$$

where $\vec{V}$, $\vec{\omega}$ and $\vec{a}_C$ are vectors of flow velocity, applied angular rate and Coriolis acceleration, respectively.

The deflection δ is given by the double integration of eq. (1):

$$\delta = \omega V t^2, \tag{2}$$

where t is the time required for a particle in the flow to travel from the nozzle to the sensing element. This time can be expressed as the product of the corresponding distance L and the inverse flow velocity. Thus, the expression for flow deflection is written as

$$\delta = \omega \frac{L^2}{V}. \tag{3}$$

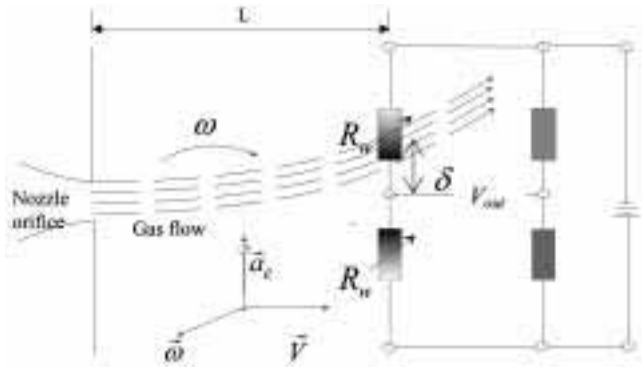

Fig. 2. Working principle of the sensor.

The deflection δ directly affects the sensitivity of the gyroscope. A larger δ causes a greater difference in the temperatures of the two opposing thermistors. Accordingly, the output voltage is higher. Equation (3) shows that gas deflection is directly proportional to the magnitude of the input angular rate. Examination of this equation also reveals other design parameters governing flow deflection, such as the effective length of the jet L and the flow velocity V. Determination of these parameters will be discussed in § 3 below.

3. Simulations and Sensitivity Analysis

Sensitivity analysis clearly shows a relationship between applied angular rate and output voltage. Based on this calculation, the sensor performance can be confirmed and optimized. For our gas gyroscope, the theoretical sensitivity is calculated by numerical simulation and is described schematically in Fig. 3.

3.1 *Flow simulation*

In this section, we discuss the gas flow regimes inside the sensing chamber and determine the positions of the thermistors so that they are in the linear velocity region during operation.

The flow must be kept within the laminar flow regime, since in this regime, the noise induced by gas flow is small and the flow itself is stable. This can be achieved by limiting the Reynolds number to sufficiently smaller than 2300, which is the critical value for in-pipe flow to become turbulent.[9] The commercial finite element model software ANSYS has been employed to simulate the flow inside the sensor using a three-dimensional model. Neon gas is introduced from the outlet of the pump; it enters the four guiding circular channels (each with a diameter of 1.3 mm) leading to the nozzle orifice to create a laminar jet flow to the sensing element. Velocity profiles of the flow from the nozzle through the sensing element to the pump chamber at six cross sections along the flow axis are shown in Fig. 4.

The Reynolds number of this model is calculated to be 205, which is the product of peak velocity, the largest diameter of the nozzle orifice and the inverse kinematic viscosity of neon gas at room temperature. This Reynolds number guarantees laminar flow inside the sensor.

The sensor detects the angular rate by converting the deflection of gas flow into the

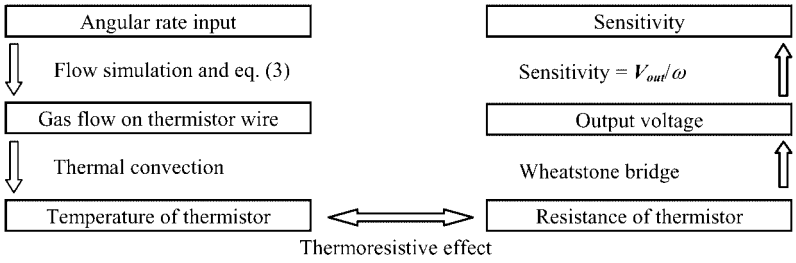

Fig. 3. Flowchart of sensitivity analysis (V_{out} is output voltage).

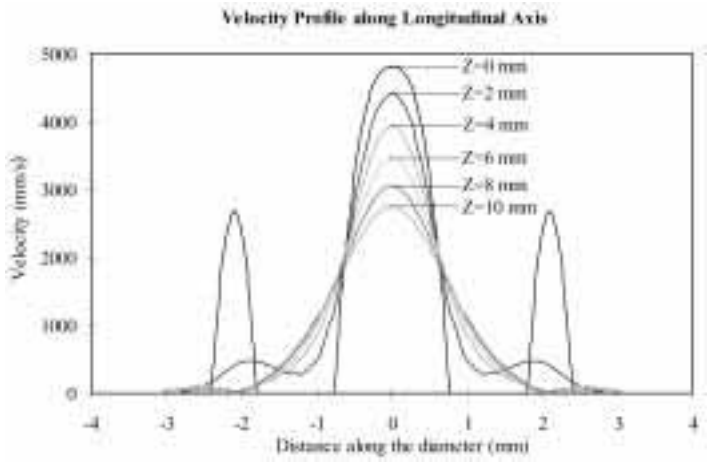

Fig. 4. Flow velocity profiles at cross sections along the sensor's longitudinal axis; *Z* is distance from the nozzle.

change in the sensing element's temperature, which depends mainly on the velocity variance of the flow reaching the thermistor. The variance of flow velocity, again, depends on the gradient of the velocity profile and the magnitude of the flow deflection. Figure 4 shows that the sensing element should be placed near the nozzle orifice so that the gradient of the flow velocity profile at the sensing plane becomes large, whereas eq. (3) shows the reverse trend for the flow deflection. In addition, the increase in distance L causes long transport times, and also reduces the frequency bandwidth, which is set at 65 Hz as the technical target for use of the sensor. Based on a consideration of these three factors, the sensing element is placed 7.5 mm from the nozzle.

On the sensing part, two thermistors are placed in opposition. The thermistor should be at the center of the linear region of gas velocity, so that the sensor can achieve the lowest nonlinearity. The gas velocity distribution at the plane of the sensing element, i.e., 7.5 mm from the nozzle, is shown in Fig. 5, and the corresponding distance between the two opposite thermistors is 1.7 mm.

3.2 *Structural simulation*

To ensure that the thermistors work well without being damaged under the gas flow conditions described above or under a shock of 3000 g, structural analysis is necessary.

The aerodynamic force acting on the thermistors may be calculated from the conventional equation for drag force on a cylinder placed in the flow,[10]

$$D = \frac{1}{2}\rho V^2 S C_{\mathrm{D}}, \tag{4}$$

where ρ, V, S and C_{D} are gas density, flow velocity, obstacle area, and the drag coefficient,

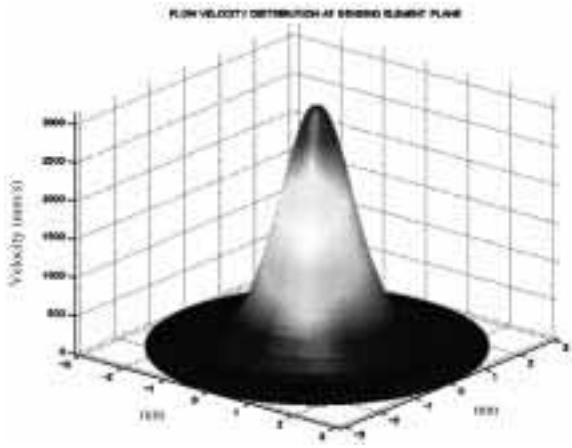

Fig. 5. Flow velocity distribution at the plane of the sensing element.

respectively. The structural analysis was carried out using ANSYS for the most extreme case of the flow peak passing through the thermistor showing a maximum stress on the thermistor of 4.57 MPa. For the shock-resistance test, an acceleration of 3000 g was applied, for which the corresponding equivalent stress on the thermistor was 2.74 MPa, guaranteeing a very high shock-resistance.

3.3 *Heat transfer and sensitivity analysis*

The heat-transfer process between the thermistor and the ambient medium is considered. The thermistor heated by a constant electrical current releases its heat to the flow and to the support arms by convection, conduction and radiation. However, the working temperature is not very high (it is designed to be less than 100°C), so thermal transfer by radiation is neglected. In addition, the effect of heat conduction between the tiny thermistor and the support arms is also often ignored.[12] Nevertheless, in the case where the support arm is not much larger than the thermist or diameter, this heat transfer should be taken into account.

For incompressible flow, and if forced convection is much larger than free convection, which is exactly the case in our sensor, heat transfer depends on only two dimensionless parameters of the flow at the thermistor: the Reynolds number and the Prandtl number.

$$Re_w = \frac{Vd}{\nu} \qquad Pr = \frac{c_p \mu}{\lambda} \tag{5}$$

Here, d, ν, μ, λ and c_p are the thermistor diameter, the kinematic viscosity, the dynamic viscosity, the thermal conductivity and the specific heat (at constant pressure) of the gas flow, respectively.

The resultant heat-transfer coefficient is defined by the Nusselt number, which is calculated using an empirical function for the specified Reynolds number from 0.4 to 4:[10]

$$Nu = 1.1C\left(\frac{Vd}{v}\right)^{n} Pr^{0.31}, \tag{6}$$

where C and n are empirical constants, the numerical values of which vary with the Reynolds number.

The amount of heat liberated per second by a thermistor of resistance R_w with constant electric current I can be deduced from I^2R_w using Joule's law. Assuming that the heat transfer is at equilibrium, the following equation can be applied:

$$I^2 R_w = \lambda \pi l\left(T_w - T_g\right)Nu. \tag{7}$$

T_w and T_g are the temperatures of the thermistor and the gas flow, respectively. When the angular rate is applied, a different flow velocity appears at the two opposing thermistors. The temperature of the thermistors changes and, as a result, their resistances change due to the thermoresistive effect:

$$R_w = R_o\left(1 + \beta T_w\right), \tag{8}$$

where β is the temperature coefficient of resistance (1/°C) and R_0 is the reference resistance of the thermistor.

Because the Wheatstone half-bridge is supplied with a constant current, the sensor response is given by:

$$V_{out} = IR_w \frac{\Delta R}{R_w}. \tag{9}$$

When the angular rate is applied, the gas deflection is calculated from eq. (3), which leads to the differential flow velocity shown in Fig. 5. After that, the heat transfer procedure and thermoresistive effect are applied until a convergent solution is obtained. Thus, the theoretical sensitivity of the sensor can be determined.

4. Fabrication and Assembly

Silicon is a highly suitable material for the sensing element, because it has a TCR larger than that of metals such as platinum and tungsten. With a suitable impurity concentration, p-type silicon can produce a TCR as large as 4800 ppm/°C.[7,8,16] On the other hand, the batch fabrication process can be utilized based on MEMS technology. Two key factors must be carefully considered and controlled during fabrication. First is the thermally induced stress in the thermistor. As the temperature in a thermistor increases or decreases, the thermistor elongates or contracts, respectively. Since the thermistors are fixed at both ends, compressive stress or tensile stress occurs within the thermistors. As a result, the resistance of the thermistor changes due to the piezoresistive effect. In this study, p-type silicon is used; hence, the thermoresistive effect in the sensing element has a positive TCR, i.e., its resistance increases when the temperature increases. However, an increase in

temperature causes a compressive stress in the thermistors; consequently, the resistance of the thermistor is reduced due to the piezoresistive effect;[13] this can cancel the resistance change due to the thermoresistive effect. To eliminate this unexpected problem, the thermistors are aligned along the <100> and <010> directions in the (001) silicon plane; they are directions in which the longitudinal piezoresistive effect is sufficiently small that it can be neglected.

The second factor that strongly affects the working characteristics of the thermistors is the concentration of impurities in silicon. This concentration is determined based on the desired TCR value and the resistance of the thermistors. In this study, it was selected to be about 5×10^{16} atoms/cm^3.

The fabrication begins with a silicon-on-insulator (SOI) wafer with a p-type device layer of 2 μm, and a resistivity of 0.5 ohm-cm. Next, 0.3-mm-thick SiO_2 is formed by thermal oxidization to create the insulating layer. The contact holes, each 2×2 μm^2 square, are opened by wet etching in BHF acid. Aluminum wires 0.3 μm thick and bonding pads are made by vacuum evaporation, photolithography and Al etching. Then, sintering is carried out to make the ohmic contact between the Al wires and the device layer through the contact holes. The thermistors are then patterned by photolithography and reactive ion etching (RIE). Finally, the structure of the thermistors is created by front and back deep reactive ion etching (DRIE). RIE is used again to remove the 0.5 μm buried SiO_2.

The fabricated sensing element is then assembled on a ceramic base using epoxy glue. To prevent thermal stress, these components are made of ceramic which has a thermal expansion coefficient value similar to that of silicon. Figure 6 shows the micrograph of the final sensing element of the gas gyroscope. The connections between the on-chip bridges to the off-chip circuit are made using gold wire, which has a diameter of 25 μm. Next, the sensing part, the nozzle orifice and the piezoelectric pump are assembled with the aluminum case. These components are fabricated by conventional machining techniques. During the assemble process, the symmetry is maintained. After neon gas is filled into the aluminum case at a pressure of 1 atm, the case is sealed. A cutout image of the gas gyroscope is shown in Fig. 7.

5. Characteristics of Sensor

Gas gyroscopes with sensing elements made of silicon (thermistor) were assembled. The TCR of the fabricated thermistor is measured as 4500 ppm/°C. The temperature of the thermistor increases as supplied current increases, as shown in Fig. 8. The parabolic form of this curve is inherited from the quadratic relation between power consumption and applied current. The mean temperature of the thermistor is set approximately 50°C higher than the ambient temperature. To attain this temperature, the applied voltage is 47 V. This temperature is selected as a compromise between sensor performance and power consumption.

To test the performance, the assembled gyroscope was placed on a turntable. The output voltage versus applied angular rate was measured with an amplification factor of 5.4, and the result is shown in Fig. 9. Theoretical results are also shown in this figure for comparison.

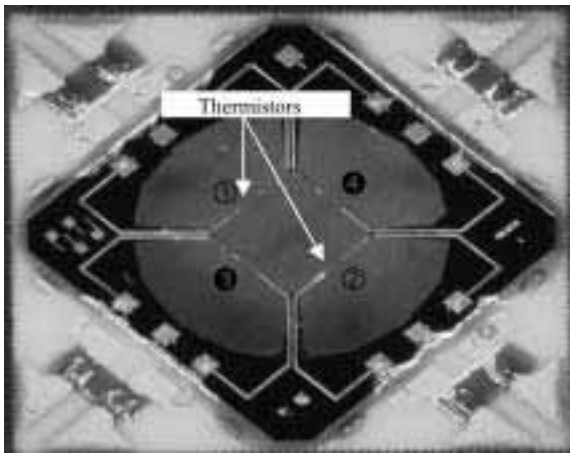

Fig. 6. Micrograph of the sensing element, where ① and ② are microthermistors, and ❸ and ❹ are reference resistors. Dimensions of thermistor are $400 \times 4 \times 2$ mm^3 (L × W × T).

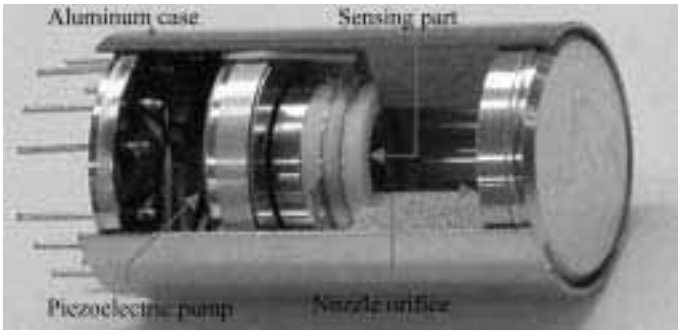

Fig. 7. Cutout view of the gyroscope; overall size is 14 mm in diameter and 25 mm in length.

The gyroscope sensitivity was 0.15 mV/°/s, which is 62 times larger than that of the gas gyroscope of the same design but with tungsten as the sensing element. Moreover, the power consumption of this gyroscope is only 5.5 mW, i.e., one-fourth of that of the tungsten one. These excellent characteristics are a result of the high TCR and high resistance of the low-doped Si thermistor. Nonlinearity smaller than 0.5% FSO has been realized. The crosstalk was measured as 0.5%. The maximum resolution based on

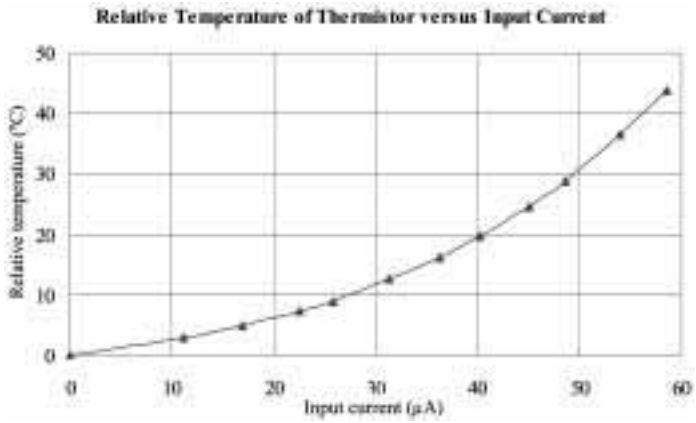

Fig. 8. Temperature of thermistor as a function of applied current.

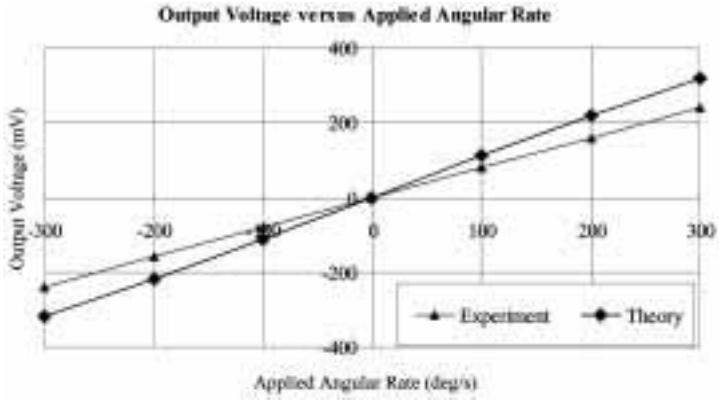

Fig. 9. Results from the silicon thermistor gyroscope.

sensitivity and noise analyses (i.e., thermal noise and 1/*f* noise in the thermistors) is 0.04 °/s.

6. Conclusions

The concept and realization of a gas gyroscope based on forced convection heat transfer and the thermoresistive effect have been presented. The configuration design, flow simulation, and structural and sensitivity analyses have been carried out and compared with experimental data. Good agreement between simulated results and experimental

results has been obtained. The semiconductor gas gyroscope has a simple configuration and should have a long performance life. The sensing element of the sensor will be further improved in the near future so that the sensor will be able to detect the dual axes of the angular rate simultaneously. This design is targeted for ship antirolling and stabilization systems.

References

1 B. Xiong, L. Che and Y. Wang: Sens. and Actuators, A **107** (2003) 137.
2 T. J. Kaiser and M. G. Allen: J. Microelectromech. Syst **12** (2003) 21.
3 C. C. Painter and A. M. Shkel: J. Micromech. Microeng. **13** (2003) 229.
4 V. Milanovic, E. Bowen, M. E. Zaghloul, N. H. Tea, J. S. Suehle, B. Payne and M. Gaitan: Appl. Phys. Lett. **76** (2000) 508.
5 S. Billat, H. Glosch, M. Kunze, F. Hedrich, J. Frech, J. Auber, H. Sandmaier, W. Wimmer and W. Lang: Sens. and Actuators, A **97-98** (2002) 125.
6 F. Mailly, A. Giani, A. Martinez, R. Bonnot, P. Temple-Boyer and A. Boyer: Sens. and Actuators, A **103** (2003) 359.
7 C. S. Fuller and J. A. Ditzenberger: J. Appl. Phys. **27** (1956) 544.
8 O. N. Tufte and E. L. Stelzer: J. Appl. Phys. **34** (1963) 313.
9 A.V. Smol'yakov and V.M Tkachenko: The Measument of Turbulent Fluctuations (Springer-Verlag, Berlin Heidelberg 1983) p. 46.
10 A. J. Chapman: Fundamentals of Heat Transfer (MacMillan, New York 1987) p. 159, p. 208
11 J. Fraden: Handbook of Modern Sensor (AIP, New York, 1997) Chap. XVI.
12 C. G. Lomas: Fundamentals of Hot Wire Anemometry (Cambridge University, 1986) Chaps II, III, IV and V.
13 D. V. Dao: Study on Silicon Piezoresistive Six DOFs Micro Forced Moment Sensors and Application to Fluid Mechanics (Doctoral Thesis, Ritsumeikan Uni., 2003) Chap. III.
14 D. D. Lee and J. W. Lim: Mems 2002 Workshop Digest (IEEE) p. 18.
15 K. D. Song, B. S. Joo, N. J. Choi, Y. S. Lee, J. S. Huh, B. K. Sohn and D. D. Lee: Proceeding of Transducer 2003 (Boston 2003) p. 520.
16 S. Sugiyama, H. Funabashi, S. Yamashita, M. Takigawa and I. Igarashi: Proc. of the 5th Sensor Symposium (Tokyo, 1986) p. 103.